Solvent-ligand Interactions Govern Stabilizing Repulsions between Colloidal Metal Oxide Nanocrystals

Charles K. Ofosu,[†] Thomas M. Truskett,[*,‡,¶] and Delia J. Milliron[*,‡,†]

†*Department of Chemistry, University of Texas at Austin, Austin, Texas 78712, United States*

‡*McKetta Department of Chemical Engineering, University of Texas at Austin, Austin, Texas 78712, United States*

¶*Department of Physics, University of Texas at Austin, Austin, Texas 78712, United States*

E-mail: truskett@che.utexas.edu; milliron@che.utexas.edu

Abstract

Nanocrystal interactions in solvent influence colloidal stability and dictate self-assembly outcomes. Small-angle X-ray scattering is used to study how dilute oleate-capped In_2O_3 nanocrystals with 7–19 nm core diameters interact when dispersed in a series of nonpolar solvents. Osmotic second virial coefficient analysis finds toluene-dispersed NCs interact like hard spheres with diameters comprising the inorganic core and a ligand-solvent corona with a core-size independent thickness. Dynamic light scattering measurements show consistent hydrodynamic and thermodynamic size scaling, further indicating hard-sphere-like behavior. By choosing solvents with stronger ligand-solvent attractions, the effective ligand-solvent corona thickness can be increased by approximately one solvent molecular diameter (0.8 nm). These results highlight the role that solvent choice could play in designing nanocrystal contact spacing, important in the initial stages of superlattice assembly or for modulating the optical response of plasmonic or photoluminescent colloidal gel networks.

Colloidal nanocrystals (NCs), nanoparticles with a crystalline inorganic core surrounded by a stabilizing interfacial layer and dispersed in layer-compatible media, exhibit distinctive and application enabling properties.[1–4] Understanding how NC interactions depend on the dispersion solvent, and properties of the NCs themselves, is essential because NCs are often synthesized, assembled, characterized, and utilized in solution.[5] For NCs dispersed in nonpolar solvents, organic ligand shells resist the compression required for two NC cores to come in close contact.[6,7] Resistance to interpenetration of ligand shells from neighboring NCs comes from the reduced ligand conformational entropy and the loss of energetically favorable solvent-ligand interactions, resulting in elastic and osmotic inter-NC repulsions, respectively, which enhance colloidal stability.[8–10] Though it is widely recognized that the solvent-ligand corona helps determine NC interactions,[9] measurements leading to a fundamental understanding of the effective pair potential remain a challenge.

Several studies have assessed characteristics that determine how dispersed NCs interact.[11–20] Kraus and coworkers investigated NCs with alkanethiol ligand shells, utilizing molecular simulation and small-angle X-ray scattering (SAXS) analysis of NC agglomeration to indirectly infer how ligand shells influence NC interactions. Their studies revealed dependencies on NC core size,[16] ligand ordering and shell structure,[16] ligand length[17] and solvent conditions.[18,19] One complicating factor of ligand shells comprising linear alkyl tails is their propensity to order if solvent quality is reduced, leading to nonuniform shell structure and anisotropic interactions. Such ligand shell changes can lead to unusual transitions in NC assemblies, e.g. anomalous NC superlattice melting upon cooling.[21,22]

Two experimental studies probed the effective isotropic pair interaction between dispersed NCs more directly by measuring their size-dependent osmotic second virial coefficient, B_2:[23,24]

$$B_2 = -2\pi \int_0^\infty \left(\exp\left[-\beta U(r)\right] - 1\right) r^2 \, dr. \tag{1}$$

Here, $U(r)$ is the NC-NC potential of mean force in the low NC concentration limit, $\beta = (k_\mathrm{B}T)^{-1}$, k_B is the Boltzmann constant, T is temperature, and r is the distance between NC centers. Saunders and Korgel studied small (2–6 nm) dodecanethiol-coated gold NCs and found a transition from net attractive ($B_2 < 0$) to repulsive ($B_2 > 0$) NC interactions as a function of core diameter.[11] These observations indicated the stabilizing repulsion provided by the ligand shell is sensitive to core curvature for NCs in this size range. Phillipse and coworkers investigated 5–12 nm diameter oleic acid–capped PbSe NCs, noting the opposite trend: interactions that crossover from net repulsive to attractive upon increasing core diameter.[12] This result was hypothesized to reflect electric multipolar attractions that originate from the interactions between NC surface ions and strengthen in proportion to NC surface area. Despite insights provided by these studies, to understand how NC pair interactions depend on NC size and solvent-ligand shell compatibility, there is a need to characterize systems free of complicating factors like strong curvature effects, propensity for strong ordering of the ligand shell, and surface-ion-induced multipolar interactions.

Here, we study interactions between highly uniform In_2O_3 NCs with 7–19 nm core diameters capped with oleate ligands, one of the most common surface ligands on colloidal NCs, by B_2 measurements using SAXS. The bent (cis) configurational isomer of oleic acid is expected to minimize anisotropic ordering of the NC ligand shell.[25–27] In_2O_3 NCs can be

synthesized with well-characterized shapes, near-isotropic interactions and narrow size distributions. Our analysis establishes that the NCs dispersed in toluene interact as hard spheres with a thermodynamic diameter reflecting the inorganic core surrounded by a core-size independent ligand-solvent corona. We further show that B_2 is sensitive to the strength of the solvent-ligand attraction, as characterized using the Flory interaction parameter. Strong attractions augment the corona thickness by up to an additional solvent layer. This sensitivity to solvent-ligand interactions suggests solvent quality can be leveraged to tune NC core-core spacings, with implications for the initial stages of superlattice assembly [20,28–30] or the optical response of assembled structures like plasmonic or photoluminescent gel networks [31–33]

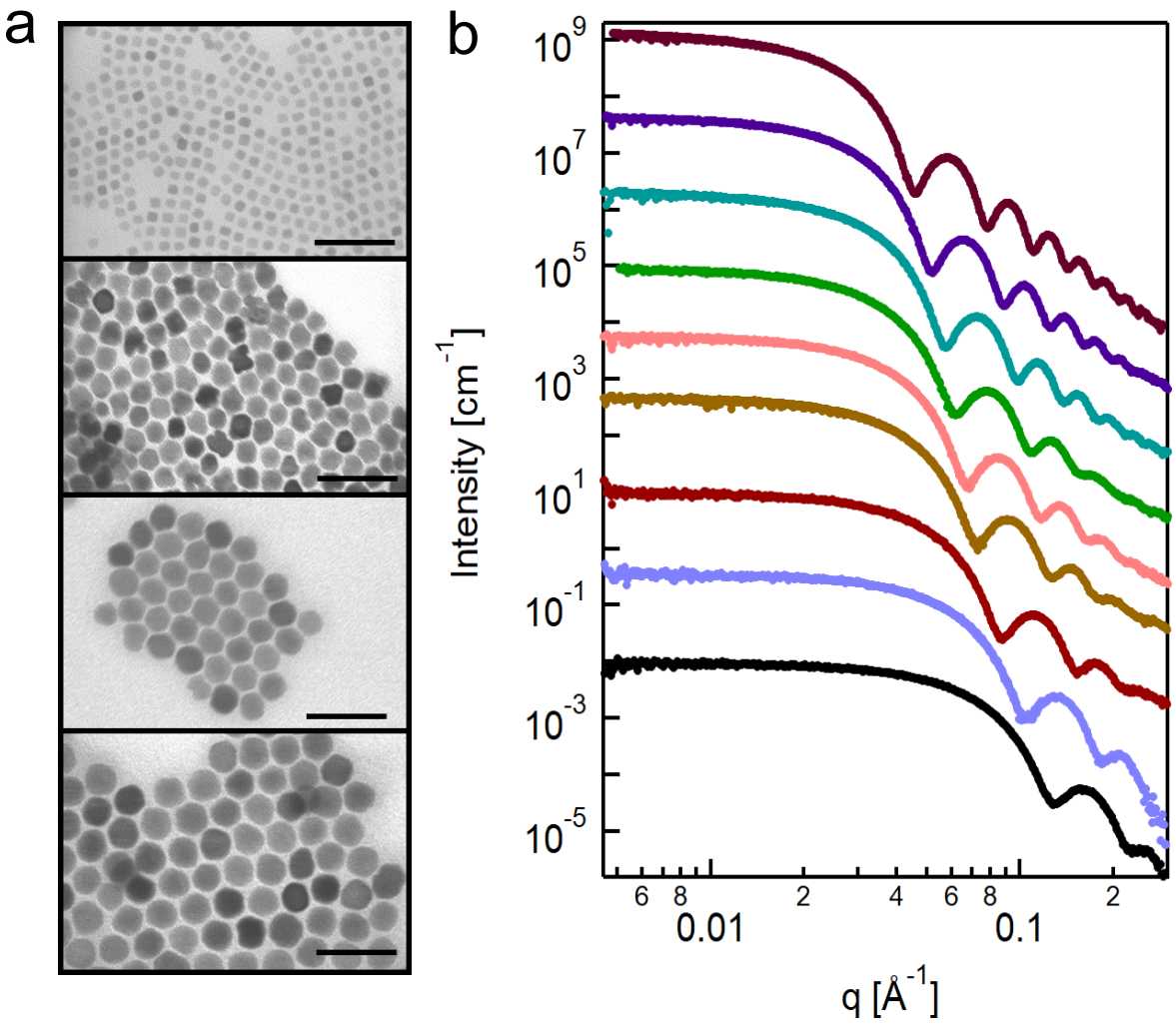

Figure 1: **Characterization of NCs**. (a) Scanning transmission electron microscope (STEM) images of D_{core} = 7.1 nm, 14.6 nm, 17.4 nm and 19.3 nm In_2O_3 NCs. Scale bars = 100 nm (b) SAXS form factors of dilute (5 mg/ml) NCs dispersed in toluene. Data have been vertically offset for clarity (D_{core} = 7.1 nm – 19.3 nm, bottom to top).

Colloidal In_2O_3 NCs were synthesized in an inert environment using a standard Schlenk line technique by following a continuous slow injection method. [1,2] The quasi-spherical mor-

phology was confirmed by bright-field scanning transition electron microscopy (STEM) (Figs. 1a and S1), and the size distributions of the NCs were estimated using SAXS (Figs. 1b and S2). The latter was accomplished by fitting a standard analytical form factor for a dilute ensemble of spherical particles of average core diameter D_{core} and a standard deviation dD_{core} to the experimental form factor $P(q)$. The form factors (Fig. 1a) show several Bessel oscillations that persist in the intermediate q regime, i.e., 0.05 Å^{-1} $< q <$ 0.2 Å^{-1}. This characteristic strongly confirms that the ligand-capped In_2O_3 NCs particles are near-spherical in shape and have a narrow size distribution (size dispersity $< 10\%$, Table S1).

In addition to providing shape information about individual NCs, SAXS also captures aspects of their spatial organization via the static structure factor, $S(q)$. The structure factor arises from the interference between X-rays scattered from multiple NC cores. We measured the scattered intensity profiles of the In_2O_3 NCs dispersed in toluene at different core volume fractions $\phi_v = \rho V_p$, where ρ is the NC number density and $V_p = \pi D_{\text{core}}^3/6$. As expected, intensity increases with ϕ_v (Fig. 2a).

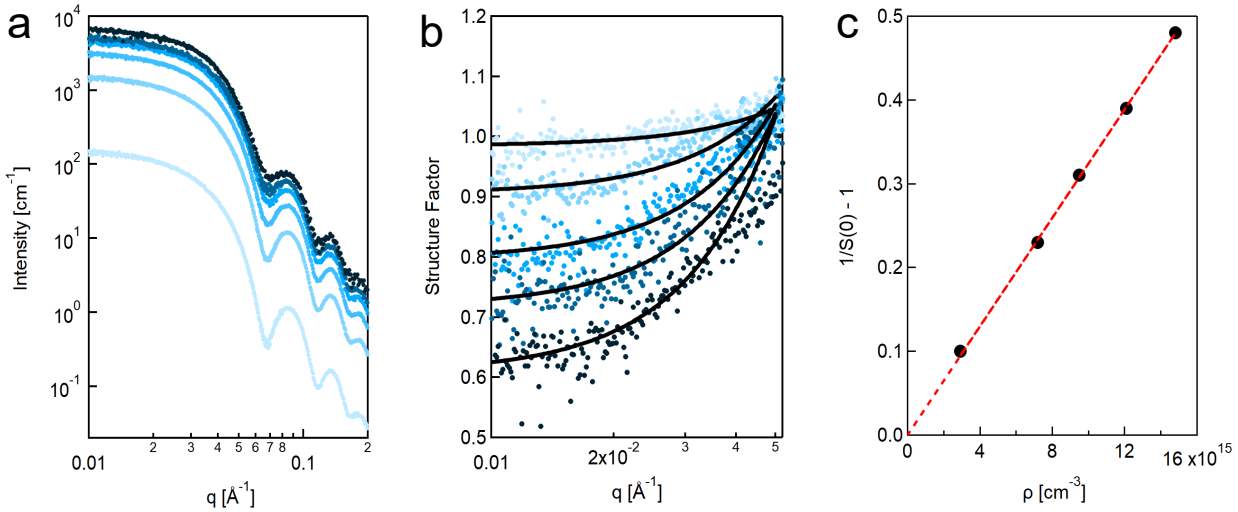

Figure 2: **Structure factor deconvolution and osmotic second virial coefficient extraction**. (a) SAXS intensity profiles for dilute dispersions of In_2O_3 NCs (D_{core} =13.5 nm, $dD_{\text{core}} = 7.6$ %) for various volume fractions ($\phi_v = 0.06$, 0.63, 1.42, 2.32, 2.92 and 4.34 v/v %, light to dark symbols) at 25 °C. (b) $S(q)$ calculated from data using Equation 2. Curves are fits of a quadratic function to low q data. (c) Reciprocal of structure factor at zero wavevector, $1/S(0)$, versus NC number density, ρ. Osmotic second virial coefficient B_2 is estimated as one half of the slope of the linear regression.

To quantitatively characterize the interactions between NCs, we determine $S(q)$ from the measured scattering intensity, which for spherical particles can be expressed as

$$I_s(q) = \frac{\phi_v}{V_p}\Delta_\rho^2 V_p^2 P(q)S(q) \tag{2}$$

Here, Δ_ρ is the scattering length density contrast between the NC core and the dispersion medium. Since $P(q)$ is independent of concentration, and $S(q) \approx 1$ as $\phi_v \to 0$, $S(q)$ can

be determined by dividing the quantity $I_s(q)/\phi_v$ by the same quantity measured in a dilute dispersion. As NC concentration increases, $S(q)$ deviates from unity in the Guinier ($q < 0.05$ Å^{-1}) region due to increased interaction between the NCs. In repulsive NC systems, $S(q) < 1$, whereas $S(q) > 1$ signifies net attractions. For these oleate-capped In_2O_3 NCs, $S(q)$ at low q monotonically decreased with increasing concentration, indicating dominant repulsive interactions (Fig. 2b).

Deconvolution of $S(q)$ from the measured intensity is the basis for accurately extracting B_2. Since the quantity $S(0)^{-1}$ is proportional to the osmotic compressibility, one can relate it to B_2 through a virial expansion of the osmotic pressure truncated at the second term,[24]

$$\frac{1}{S(0)} = 1 + 2B_2\rho + \mathcal{O}\left(\rho^2\right) \tag{3}$$

Given that the structure factor varies proportional to q^2 near $q = 0$, $S(0)$ for each of the low NC concentration samples can be obtained by fitting a quadratic function to the structure factor data in the low q region (Fig. 2b). The osmotic second virial coefficient B_2 is then estimated as one half of the slope of the linear regression of $S(0)^{-1}$ versus ρ (Fig. 2c). A wide range of NC sizes can be synthesized and D_{core} is an essential parameter for tuning the properties of individual NCs[34] and their assemblies.[35] To investigate how the size of the inorganic core and the ligand-solvent corona impact the effective interparticle interactions, we measured B_2 for a series of NC core sizes ranging from 7.1 nm to 19.3 nm. The measured osmotic second virial coefficient increases monotonically with core size, qualitatively similar to the expected trend for hard-sphere-like colloids (Fig. S4 and Table S1). However, the magnitudes of B_2 are larger, and increase more rapidly with D_{core}, than predicted for hard spheres with the core diameter (Fig. 3a). To ascertain whether the primary effect of the solvent-ligand corona is to augment the core diameter by a constant amount, we fit the following expression to the experimental B_2 data:

$$B_2^{\text{HS}} = \frac{2\pi}{3}\left(D_{\text{core}} + 2t_{\text{shell}}\right)^3 \tag{4}$$

The measured virial coefficients are remarkably consistent with this simple model with a fixed solvent-ligand shell thickness $t_{\text{shell}} = 2.03 \pm 0.15$ nm, i.e., NCs with an effective thermodynamic diameter of $D_{\text{thermo}} = D_{\text{core}} + 4.06$ nm. This shell thickness is approximately equal to the sum of the oleate ligand shell thickness, as measured using small-angle neutron scattering (1.5–1.6 nm),[36,37] and one intermolecular spacing in liquid toluene, consistent with its density and neutron scattering analysis (0.6 nm).[38] The observed size dependence contrasts with the non-monotonic trends in B_2 found in earlier studies that necessitated the consideration of more complex inter-NC potentials with competing attractive and repulsive interactions and multiple fit parameters.[11,12] Likewise, attractive square-well and sticky-sphere potentials have been required to model SAXS and neutron scattering results to extract the effective B_2 and ligand shell thickness for materials whose interactions exhibit similar complexities.[15,20] The simpler, hard-sphere like behavior of the materials studied here allows extraction of effective ligand shell thickness more directly from SAXS.

Another common measure of particle size is the apparent hydrodynamic diameter D_{H}, i.e., the diameter of a Brownian hard sphere that would have the same translational dif-

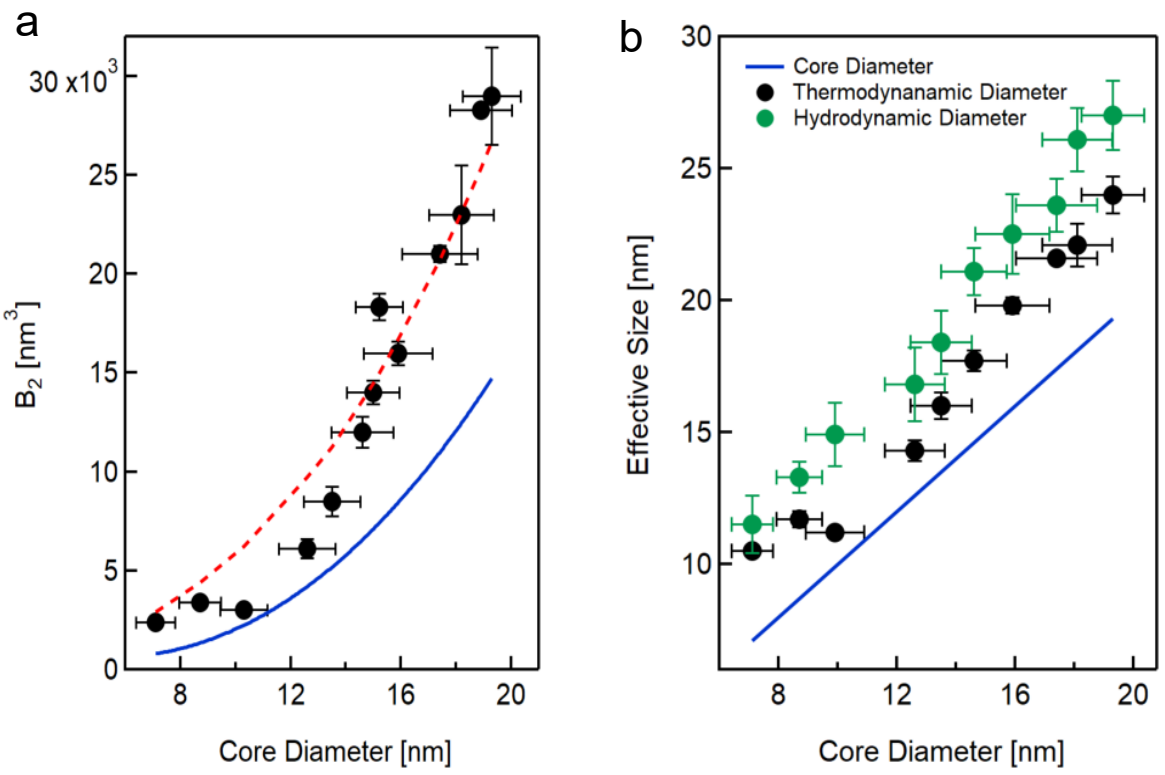

Figure 3: **Osmotic second virial coefficient size series and thermodynamic versus hydrodynamic diameters**. (a) B_2 versus NC core diameter. Solid curve is B_2^{HS} evaluated with Equation 6 using the NC core diameter (assuming $t_{\mathrm{shell}} = 0$). Circles represent experimental B_2 values and dashed curve is a fit of Equation 6 to the data, yielding $t_{\mathrm{shell}} = 2.03 \pm 0.15$ nm. (b) Comparison of the core (D_{core}), effective thermodynamic ($D_{\mathrm{thermo}} = D_{\mathrm{core}} + 2t_{\mathrm{shell}}$), and apparent hydrodynamic (D_{H}) diameters. The lateral error bars in both panels indicate the standard deviation of core sizes, dD_{core}.

fusivity as the particle of interest in a continuum fluid with the solvent's shear viscosity and temperature. Though identical for monodisperse hard spheres, quantitative correspondence between hydrodynamic and thermodynamic diameters is not generally expected or observed for other colloids. The former is a dynamically derived measure of average colloid size, while the latter reflects how interactions between colloid pairs contribute to osmotic pressure. Here, a comparison of these measures for the entire size series of oleate-capped In_2O_3 NCs in toluene may give further insight into how similar their thermodynamic and dynamic behaviors are to those of the idealized hard-sphere model.

To compare to thermodynamic diameters obtained from the B_2 analysis using SAXS (Fig. 3a and Table S1), we estimated D_{H} from dynamic light scattering (DLS) measurements of dilute NC dispersions. To this end, diffusion coefficients were extracted from the short-time decay of the intensity autocorrelation functions (Figure S5) using a third-order cumulant analysis. The intensity weighted harmonic mean hydrodynamic diameter was determined using the Stokes-Einstein equation (Table S2).[3] The size scaling of the hydrodynamic diameters show remarkably good agreement with that of the thermodynamic sizes

measured from B_2, with only a slight systematic offset to higher values (Fig. 3b).

To test sensitivity of the NC interactions to solvent choice, we prepared oleate-capped In_2O_3 NCs dispersed in a series of nonpolar solvents. The solvent-ligand interactions are characterized using the Flory χ parameter,[39,40] estimated by a solubility based approach summing enthalpic and entropic contributions, respectively:[16,41,42]

$$\chi = \beta V_S(\delta_L - \delta_S)^2 + 0.34 \tag{5}$$

Here V_S is the molecular volume of the solvent; δ_S and δ_L are the Hildebrand solubility parameters of the solvent and ligand molecules, respectively (Table 1). Despite its known limitations, e.g., for modeling alkanethiol ligand shells prone to ordering,[16] Flory-Huggins polymer solution theory provides a simple, phenomenological estimate for the strength of solvent interactions with ligands or adsorbed polymers on the surfaces dispersed colloids.[6,7,16,41,42]

Solubility parameters capture the cohesive energy density of solvent and ligand molecules in their pure condensed phases. Large differences (i.e., χ values significantly above 0.5) indicate thermodynamically unfavorable mixing and solvents incompatible with NC dispersion. At the other extreme, $\chi \approx 0.34$ predicts strong ligand-solvent attractions and hence NC-NC repulsions. The nonpolar solvents chosen for this work (Table 1) fully disperse the oleate-capped In_2O_3 NCs and lead to Flory parameters in the range $0.341 \leq \chi \leq 0.652$, including three that interact more favorably with oleate ligands than toluene (xylene, cyclohexane, and 1-octadecene), and three with relatively weaker ligand-solvent attractions (hexadecane, octane, and hexane).

Table 1: Molar volume,[43] and solubility parameters ($\delta = \delta_S$)[43] for solvents in this study, and their corresponding Flory parameter (χ) calculated via Equation 5, and sizes [$D_S = (\frac{V_s}{N_A})^{1/3}$]. Given only the aliphatic tail of the oleate ligands interact with the solvent, the ligand properties and solubility parameter ($\delta = \delta_L$) were approximated using values for cis-9-octadecene.[19]

	V_S (cm^3/mol)	δ (MPa$^{1/2}$)	χ	D_S (nm)
1-octadecene	320.0	17.4	0.341	0.8
cyclohexane	108.7	16.8	0.352	0.6
xylene	121.2	18.1	0.369	0.6
toluene	106.8	18.2	0.373	0.6
hexadecane	294.1	16.4	0.441	0.8
octane	163.5	15.6	0.536	0.6
hexane	131.6	14.9	0.652	0.6
cis-9-octadecene	316.8	17.3	–	–

** δ for cis-9-octadecene and 1-octadecene were calculated as the square root of the cohesive energy density, with their energies of vaporization obtained from the NIST Chemistry WebBook[44]

Measured structure factors of the oleate-capped In_2O_3 NCs—dispersed at 200 mg/ml in the following solvents: hexane, octane, toluene, xylene and cyclohexane—show a progressive reduction from unity in the Guinier region with decreasing χ (Fig. 4a). This trend indicates that stronger ligand-solvent attractions lead to more repulsive NC-NC pair interactions, further substantiating our interpretation of the manner in which the ligand-solvent corona

contributes to the NC thermodynamic size. The data allow us to further estimate how t_{shell} varies with χ, following the approach illustrated by Figs. 2 and 3. Varying solvents from high to low χ increases the effective thickness of ligand-solvent corona and hence the closest approach of NC cores. The only notable deviation from the trend is hexadecane versus toluene, which can be explained by the former having a significantly larger solvent molecular diameter than the latter, giving rise to a thicker ligand-solvent corona. Strikingly, these data establish that by varying solvents in this series from toluene to 1-octadecene, all within the range considered good solvents for oleate-capped NCs, one observes an increase in t_{shell} of 0.8 nm and in the core-core separation of 1.6 nm. Thus, even for NCs with effective hard-sphere-like NC-NC interactions, solvent-ligand interactions are a design parameter that can be used for substantially tuning the "contact" separation between inorganic cores. Besides their importance for maintaining stable dispersions, such interactions are thought to influence NC assembly pathways, ultimately guiding the structure of superlattices.[20,28–30]

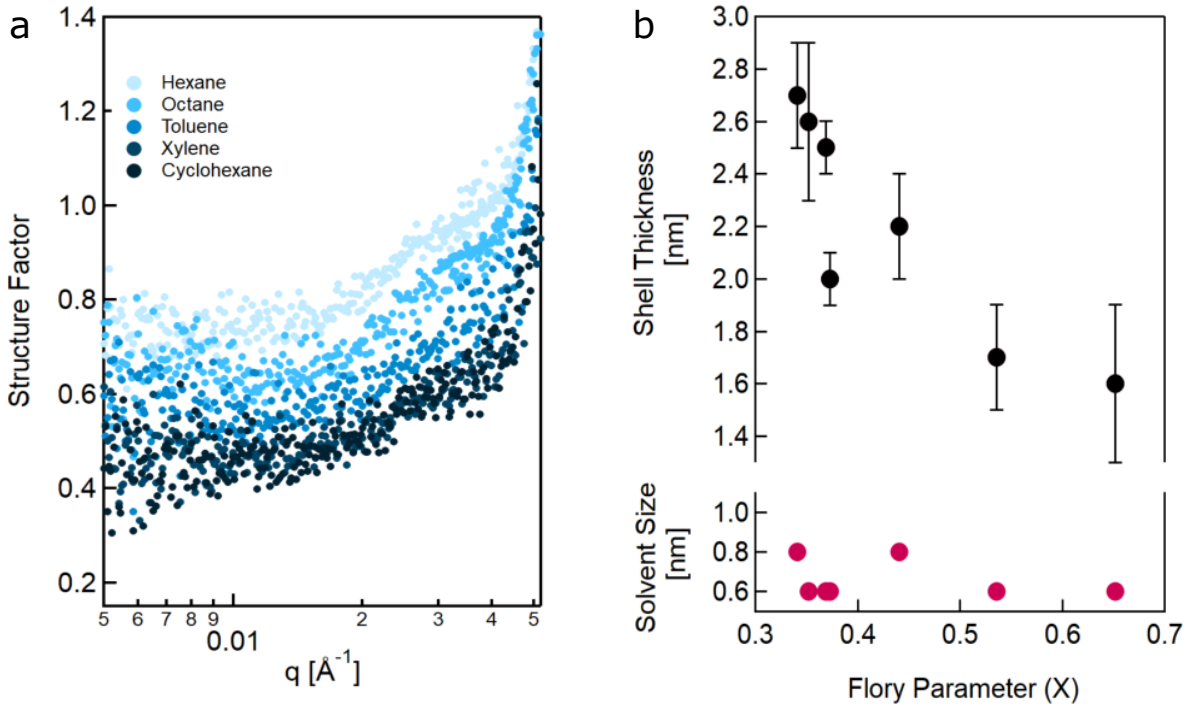

Figure 4: **Solvent influence on the effective pair interaction**. (a) Measured structure factors for oleate-capped In_2O_3 NCs (D_{core} = 16.0 nm) dispersed at 200 mg/ml in five different solvents. The solvent-ligand affinity increases as hexane < octane < toluene < xylene < cyclohexane, according to their Flory χ parameters (Table 1). (b) Ligand shell thickness t_{shell} and solvent size D_S versus χ for NCs (D_{core} = 16.0 nm) dispersed in solvents of Table 1 determined from measured $S(q)$ using the method illustrated in Figs. 2 and 3.

To summarize, we characterized the effects of core size and and solvent-ligand interactions on the osmotic second virial coefficient of oleate-capped In_2O_3 colloidal NCs using SAXS. Measurements for a size series of NCs with 7–19 nm core diameters dispersed in toluene established that NCs interact as hard spheres with an effective thermodynamic diameter comprising the core diameter plus a ligand-solvent corona with NC size-independent thickness.

The corona thickness approximately corresponded to the height of the oleate ligand shell plus a solvent molecule diameter. DLS measurements revealed consistent thermodynamic and hydrodynamic diameters, further indicating hard-sphere-like behavior. Measurements for a series of solvents demonstrated that the thermodynamic diameter, and hence the contact separation of the inorganic cores, could increase by approximately two solvent diameters when strong ligand-solvent interactions are present.

Broadly, these results suggest new opportunities for using SAXS to systematically characterize, understand, and design interactions between functional nanoscale colloids. In particular, we envision using solvent-ligand interactions to tune or even dynamically modulate core-core spacings, and hence optical response, of plasmonic or photoluminescent colloidal gel assemblies.[31–33]

Experimental Methods

In_2O_3 NCs were synthesized by modification of methods published by the Hutchison group.[1,2] Here, a prepared indium oleate-acetate precursor solution was injected into a hot (290 °C) oleyl alcohol bath via a slow injection procedure. The injection volume determined the size of the inorganic NC cores. Electron microscopy was performed on a Hitachi S5500 STEM instrument to confirm the morphology. Samples were drop-cast on Type-A ultrathin carbon copper TEM grids (Ted Pella, 01822, 400 mesh) from dilute NCs dispersions in hexane.

SAXS measurements were performed in transmission configuration with a sample-to-detector distance of 1.085 m on a SAXSLAB Ganesha instrument using Cu Kα radiation. Dilute NC dispersions were enclosed in flame-sealed glass capillaries (Charles-Supper Company, Boron Rich, 1.5 mm diameter, 0.01 mm wall thickness). A capillary containing neat solvent only was used for background subtraction. Scattering patterns were calibrated using a silver (I) behenate standard and were converted into 1D data by circular averaging using the Igor Pro-based Nika software. The intensity profiles of the most dilute dispersions were fitted with the equation for the form factor of spherical particles with a Gaussian size distribution to determine the NC size and size distribution.

DLS measurements of dilute NCs ($1-2$ mg/mL) were performed using a Zetasizer Nano ZS (Malvern) equipped with a He-Ne laser ($\lambda = 633$ nm) and 173° detection optics. Sample cell temperature was kept at 25 °C. Measured autocorrelation functions in triplicate, each with an acquisition time of 10 s, were averaged. NC hydrodynamic sizes and their respective standard deviations were calculated from the first and second cumulant terms of a polynomial fit to the averaged autocorrelation curves.[3]

Acknowledgement

This work was primarily supported by the National Science Foundation through the Center for Dynamics and Control of Materials: an NSF Materials Research Science and Engineering Center (NSF MRSEC) under Cooperative Agreement DMR-1720595. This work was also supported by the Welch Foundation (F-1848 and F-1696). SAXS data was collected at UT Austin with an instrument acquired under NSF MRI grant (CBET-1624659). The authors

acknowledge help with the graphical abstract from D. Davies and helpful discussions with Z. M. Sherman, A. M. Green, J. Ilavsky, and S. Barton.

Supporting Information Available

Further experimental details and additional data for the synthesis of oleate-capped In_2O_3 NCs and their characterization by STEM, SAXS, and DLS are presented in the supporting information.

References

(1) Agrawal, A.; Cho, S. H.; Zandi, O.; Ghosh, S.; Johns, R. W.; Milliron, D. J. Localized Surface Plasmon Resonance in Semiconductor Nanocrystals. *Chem. Rev.* **2018**, *118*, 3121–3207.

(2) Alivisatos, A. P. Semiconductor Clusters, Nanocrystals, and Quantum Dots. *Science* **1996**, *271*, 933.

(3) Talapin, D. V.; Lee, J.-S.; Kovalenko, M. V.; Shevchenko, E. V. Prospects of Colloidal Nanocrystals for Electronic and Optoelectronic Applications. *Chem. Rev.* **2010**, *110*, 389–458.

(4) Shamsi, J.; Urban, A. S.; Imran, M.; De Trizio, L.; Manna, L. Metal Halide Perovskite Nanocrystals: Synthesis, Post-Synthesis Modifications, and Their Optical Properties. *Chem. Rev.* **2019**, *119*, 3296–3348.

(5) Mattoussi, H.; Cumming, A. W.; Murray, C. B.; Bawendi, M. G.; Ober, R. Characterization of CdSe Nanocrystallite Dispersions by Small Angle X-ray Scattering. *J. Chem. Phys.* **1996**, *105*, 9890–9896.

(6) Vincent, B.; Edwards, J.; Emmett, S.; Jones, A. Depletion Flocculation in Dispersions of Sterically-Stabilised Particles ("Soft Spheres"). *Colloids Surf.* **1986**, *18*, 261–281.

(7) Shah, P. S.; Holmes, J. D.; Johnston, K. P.; Korgel, B. A. Size-Selective Dispersion of Dodecanethiol-Coated Nanocrystals in Liquid and Supercritical Ethane by Density Tuning. *J. Phys. Chem. B* **2002**, *106*, 2545–2551.

(8) Heuer-Jungemann, A.; Feliu, N.; Bakaimi, I.; Hamaly, M.; Alkilany, A.; Chakraborty, I.; Masood, A.; Casula, M. F.; Kostopoulou, A.; Oh, E.; Susumu, K.; Stewart, M. H.; Medintz, I. L.; Stratakis, E.; Parak, W. J.; Kanaras, A. G. The Role of Ligands in the Chemical Synthesis and Applications of Inorganic Nanoparticles. *Chem. Rev.* **2019**, *119*, 4819–4880.

(9) Boles, M. A.; Ling, D.; Hyeon, T.; Talapin, D. V. The Surface Science of Nanocrystals. *Nat. Mater.* **2016**, *15*, 141–153.

(10) Calvin, J. J.; Brewer, A. S.; Alivisatos, A. P. The Role of Organic Ligand Shell Structures in Colloidal Nanocrystal Synthesis. *Nat. Synth.* **2022**, *1*, 127–137.

(11) Saunders, A. E.; Korgel, B. A. Second Virial Coefficient Measurements of Dilute Gold Nanocrystal Dispersions Using Small-Angle X-ray Scattering. *J. Phys. Chem. B* **2004**, *108*, 16732–16738.

(12) van Rijssel, J.; Peters, V. F. D.; Meeldijk, J. D.; Kortschot, R. J.; van Dijk-Moes, R. J. A.; Petukhov, A. V.; Erné, B. H.; Philipse, A. P. Size-Dependent Second Virial Coefficients of Quantum Dots from Quantitative Cryogenic Electron Microscopy. *J. Phys. Chem. B* **2014**, *118*, 11000–11005.

(13) Grest, G. S.; Wang, Q.; in't Veld, P.; Keffer, D. J. Effective Potentials Between Nanoparticles in Suspension. *J. Chem. Phys.* **2011**, *134*, 144902.

(14) Yadav, H. O. S.; Shrivastav, G.; Agarwal, M.; Chakravarty, C. Effective Interactions Between Nanoparticles: Creating Temperature-Independent Solvation Environments for Self-Assembly. *J. Chem. Phys.* **2016**, *144*, 244901.

(15) Schroer, M. A.; Schulz, F.; Lehmkuhler, F.; Moller, J.; Smith, A. J.; Lange, H.; Vossmeyer, T.; Grubel, G. Tuning the Interaction of Nanoparticles from Repulsive to Attractive by Pressure. *J. Phys. Chem. C* **2016**, *120*, 19856–19861.

(16) Kister, T.; Monego, D.; Mulvaney, P.; Widmer-Cooper, A.; Kraus, T. Colloidal Stability of Apolar Nanoparticles: The Role of Particle Size and Ligand Shell Structure. *ACS Nano* **2018**, *12*, 5969–5977.

(17) Monego, D.; Kister, T.; Kirkwood, N.; Mulvaney, P.; Widmer-Cooper, A.; Kraus, T. Colloidal Stability of Apolar Nanoparticles: Role of Ligand Length. *Langmuir* **2018**, *34*, 12982–12989.

(18) Doblas, D.; Kister, T.; Cano-Bonilla, M.; González-García, L.; Kraus, T. Colloidal Solubility and Agglomeration of Apolar Nanoparticles in Different Solvents. *Nano Lett.* **2019**, *19*, 5246–5252.

(19) Monego, D.; Kister, T.; Kirkwood, N.; Doblas, D.; Mulvaney, P.; Kraus, T.; Widmer-Cooper, A. When Like Destabilizes Like: Inverted Solvent Effects in Apolar Nanoparticle Dispersions. *ACS Nano* **2020**, *14*, 5278–5287.

(20) Winslow, S. W.; Liu, Y.; Swan, J. W.; Tisdale, W. A. Repulsive, Densely Packed Ligand-Shells Mediate Interactions between PbS Nanocrystals in Solution. *J. Phys. Chem. C* **2021**, *125*, 8014–8020.

(21) Yu, Y.; Jain, A.; Guillaussier, A.; Voggu, V. R.; Truskett, T. M.; Smilgies, D.-M.; Korgel, B. A. Nanocrystal Superlattices that Exhibit Improved Order on Heating: An Example of Inverse Melting? *Faraday Discuss.* **2015**, *181*, 181–192.

(22) Yu, Y.; Guillaussier, A.; Voggu, V. R.; Pineros, W.; Truskett, T. M.; Smilgies, D.-M.; Korgel, B. A. Cooling Dodecanethiol-Capped 2 nm Diameter Gold Nanocrystal Superlattices below Room Temperature Induces a Reversible Order–Disorder Structure Transition. *J. Phys. Chem. C* **2016**, *120*, 27682–27687.

(23) Zimm, B. H. The Scattering of Light and the Radial Distribution Function of High Polymer Solutions. *J. Chem. Phys.* **1948**, *16*, 1093–1099.

(24) Vrij, A.; Tuinier, R. In *Particulate Colloids*; Lyklema, J., Ed.; Fundamentals of Interface and Colloid Science; Academic Press, 2005; Vol. 4; pp 5–1–5–103.

(25) Yang, Y.; Qin, H.; Jiang, M.; Lin, L.; Fu, T.; Dai, X.; Zhang, Z.; Niu, Y.; Cao, H.; Jin, Y.; Zhao, F.; Peng, X. Entropic Ligands for Nanocrystals: From Unexpected Solution Properties to Outstanding Processability. *Nano Lett.* **2016**, *16*, 2133–2138.

(26) Balan, A. D.; Olshansky, J. H.; Horowitz, Y.; Han, H.-L.; O'Brien, E. A.; Tang, L.; Somorjai, G. A.; Alivisatos, A. P. Unsaturated Ligands Seed an Order to Disorder Transition in Mixed Ligand Shells of CdSe/CdS Quantum Dots. *ACS Nano* **2019**, *13*, 13784–13796.

(27) Elimelech, O.; Aviv, O.; Oded, M.; Peng, X.; Harries, D.; Banin, U. Entropy of Branching Out: Linear versus Branched Alkylthiols Ligands on CdSe Nanocrystals. *ACS Nano* **2022**, *16*, 4308–4321.

(28) Lee, B.; Littrell, K.; Sha, Y.; Shevchenko, E. V. Revealing the Effects of the Nonsolvent on the Ligand Shell of Nanoparticles and Their Crystallization. *J. Am. Chem. Soc.* **2019**, *141*, 16651–16662.

(29) Bian, K.; Choi, J. J.; Kaushik, A.; Clancy, P.; Smilgies, D.-M.; Hanrath, T. Shape-Anisotropy Driven Symmetry Transformations in Nanocrystal Superlattice Polymorphs. *ACS Nano* **2011**, *5*, 2815–2823.

(30) Weidman, M. C.; Smilgies, D.-M.; Tisdale, W. A. Kinetics of the Self-Assembly of Nanocrystal Superlattices Measured by Real-Time In Situ X-ray Scattering. *Nature Mater.* **2016**, *15*, 775–781.

(31) Saez Cabezas, C. A.; Ong, G. K.; Jadrich, R. B.; Lindquist, B. A.; Agrawal, A.; Truskett, T. M.; Milliron, D. J. Gelation of Plasmonic Metal Oxide Nanocrystals by Polymer-Induced Depletion Attractions. *Proc. Natl. Acad. Sci. USA* **2018**, *115*, 8925–8930.

(32) Singh, M.; Sherman, Z. M.; Milliron, D. J.; Truskett, T. M. Linker-templated structure tuning of optical response in plasmonic nanoparticle gels. *ChemRxiv* **2022**, 10.26434/chemrxiv–2022–fvcnb.

(33) Green, A. M.; Ofosu, C. K.; Kang, J.; Anslyn, E. V.; Truskett, T. M.; Milliron, D. J. Assembling Inorganic Nanocrystal Gels. *Nano Lett.* **2022**, *22*, 1457–1466.

(34) Grassian, V. H. When Size Really Matters: Size-Dependent Properties and Surface Chemistry of Metal and Metal Oxide Nanoparticles in Gas and Liquid Phase Environments. *J. Phys. Chem. C* **2008**, *112*, 18303–18313.

(35) Kao, J.; Bai, P.; Lucas, J. M.; Alivisatos, A. P.; Xu, T. Size-Dependent Assemblies of Nanoparticle Mixtures in Thin Films. *J. Am. Chem. Soc.* **2013**, *135*, 1680–1683.

(36) Toolan, D. T.; Weir, M. P.; Allardice, J.; Smith, J. A.; Dowland, S. A.; Winkel, J.; Xiao, J.; Zhang, Z.; Gray, V.; Washington, A. L.; Petty II, J. E., Anthony J. Anthony; Greenham, N. C.; Friend, R. H.; Rao, A.; Jones, R. A. L.; Ryan, A. J. Insights into the Structure and Self-Assembly of Organic-Semiconductor/Quantum-Dot Blends. *Adv. Funct. Mater.* **2022**, *32*, 2109252.

(37) Weir, M. P.; Toolan, D. T.; Kilbride, R. C.; Penfold, N. J.; Washington, A. L.; King, S. M.; Xiao, J.; Zhang, Z.; Gray, V.; Dowland, S.; Winkel, J.; Greenham, N. C.; Friend, R. H.; Rao, A.; Ryan, A. J.; Jones, R. A. L. Ligand Shell Structure in Lead Sulfide–Oleic Acid Colloidal Quantum Dots Revealed by Small-Angle Scattering. *J. Phys. Chem. Lett.* **2019**, *10*, 4713–4719.

(38) Falkowska, M.; Bowron, D. T.; Manyar, H. G.; Hardacre, C.; Youngs, T. G. Neutron Scattering of Aromatic and Aliphatic Liquids. *ChemPhysChem* **2016**, *17*, 2043–2055.

(39) Flory, P. J. Thermodynamics of High Polymer Solutions. *J. Chem. Phys.* **1942**, *10*, 51–61.

(40) Flory, P. J. *Principles of Polymer Chemistry*; Cornell University Press, 1953.

(41) Raghavan, S. R.; Hou, J.; Baker, G. L.; Khan, S. A. Colloidal Interactions Between Particles with Tethered Nonpolar Chains Dispersed in Polar Media: Direct Correlation Between Dynamic Rheology and Interaction Parameters. *Langmuir* **2000**, *16*, 1066–1077.

(42) Khan, S. J.; Pierce, F.; Sorensen, C.; Chakrabarti, A. Self-Assembly of Ligated Gold Nanoparticles: Phenomenological Modeling and Computer Simulations. *Langmuir* **2009**, *25*, 13861–13868.

(43) Brandrup, J.; Immergut, E. H.; Grulke, E. A. *Polymer Handbook*; Wiley: New York, 1999.

(44) NIST Chemistry WebBook, SRD 69. `https://webbook.NIST.gov/chemistry/`.

TOC Graphic